Distributed Robust Scheduling for a Virtual Power Plant with Uncertain Renewable Generations Considering Integrated Demand Response

111[1], 111[1], 111[2⋆], and 111[3]

[1] Beijing Institute for Scientific and Engineering Computing, Beijing University of Technology, Beijing 100124, P.R. China.
[2]

Abstract. The adverse effects of fossil fuels on the environment have greatly accelerated the combination of multiple energy systems. A comprehensive energy system can be oriented towards different spatial scales such as parks, towns, and cities, to couple different types of energy supply systems. They enable the coordinated supply of electricity, cooling, and other forms of energy, resulting in improved environmental and economic benefits. This study aims to explore the effective management of distributed renewable energy in multi-user park-level integrated energy system (PIES). Considering the effect of photovoltaic (PV) systems and loads uncertainty on virtual power plant (VPP) scheduling, a two-stage robust optimization model based on integrated demand response for VPP is proposed.

Keywords: Virtual power plant (VPP), Production task scheduling, Park-level integrated energy system (PIES), Distributionally robust optimization, Scenario generation

1 Introduction

Industrial park (or industrial estate) is an area planned for industrial development, usually with a large energy demand, especially for electricity. Industrial production is closely related to energy demand, and its development brings economic benefits while also exacerbating environmental challenges, such as the climate change crisis, improving sustainability and energy efficiency. Faced with the challenge of climate change, policies such as carbon reduction and carbon neutrality have become a consensus among countries. These policies aim to address climate change by reducing greenhouse gas emissions and achieving a state of net-zero emissions through measures such as mitigation and offsetting.

Due to environmental benefits, renewable energy sources (REs) such as wind energy and photovoltaic power generation systems, which can be used as potential solutions, are playing an increasingly important role in meeting electricity demand. This forces the combination of multiple energy systems to accelerate significantly to offset the adverse environmental impacts of fossil fuels. In industry, a park-level integrated energy system

⋆ Corresponding author.

(PIES) with a large number of small-scale distributed generator (DG) has been proposed to meet a variety of needs. On the one hand, it can easily realize the flexible adjustment of power distribution and provide energy for industrial users; On the other hand, it can provide a new solution to the problem of environmental pollution from the root.

DG is widely adopted for its reliability, cost-effectiveness, flexibility, and environmental benefits. However, it also poses challenges for power market management due to its small capacity, large quantity, and uneven distribution. Additionally, the intermittent and stochastic nature of DG generation further complicates the management of power systems. Virtual power plant (VPP), it emerged as an important means to ensure stable operation of the power system and achieve efficient utilization and sharing of energy resources. Through advanced communication technology and software systems, it participates in the power market and grid operation as a special power plant, thereby aggregating and optimizing various distributed energy sources.

The study of real-time scheduling of VPP is essential because the output of intermittent renewable energy has strong fluctuation characteristics. The uncertainty in wind and solar power output, along with load forecasting, results in a lack of accurate decision-making basis for scheduling and operating VPP systems, leading to significant economic losses. The significant uncertainty of WP, PV, and load means that traditional deterministic optimization methods are no longer sufficient for VPP scheduling [3], leading scholars to primarily focus on uncertainty optimization problems (Kong et al., 2020). Kuang et al. (2019) and Budiman et al. (2022) quantified random variables as scenarios through stochastic optimization, and the optimal scheduling solution is obtained based on the operating results under different scenarios. Lu et al. (2015) employed a stochastic-constrained optimization method to develop a scheduling model that considers various uncertainties, including renewable energy sources and load.

Another widely-used DR approach is to install battery storage assets in industrial park. Battery storage can store electric energy during low-price periods and release the stored electricity to supply users during high-price periods.

Currently, some scholars have already discussed the uncertainties in integrated electricity and natural gas energy systems

For partial surveys, see, e.g. [**?**,**?**,**?**,**?**,**?**,**?**]. Here, it is assumed that for any two input points from a metric space a pair-wise distance can be computed that reflects their dissimilarity. $\mathbf{p}(n, m)$ $p(n, m)$

An IDR-based energy hub program is proposed in [13], whereby the electricity is switched to natural gas during peak hours.

To characterize the interest relationship between the entities in the energy transaction process, many scholars have studied MCIESs based on game theory [14-17].

Table 1 summarizes the main differences between the proposed model in our work and the most relevant research studies in the field.

the demand response is considered to be a key and effective measure to stimulate the interaction between demand-side resources and renewable energy, but the demand response potential of building users has not been fully explored.

In response to these problems, this study investigated a hierarchical stochastic scheduling method based on a Stackelberg game in an uncertain environment. Compared with

the existing research, the main innovations and contributions of this paper are as follows.

Generative adversarial network (GAN) [4] is a group of novel generative model which has received extensive attention in recent years. Broad areas of GAN applications are increasing quickly with time and it has been emerged in 3D object generation, medicine, pandemics, image processing, face detection, texture transfer, and traffic controlling [12]. Undoubtedly, deep learning associated on GAN has presenting remarkable outcomes on these fields. The basic idea of GAN deployment is for unsupervised machine learning techniques, which consist of two different and competing networks: a generative model and a discriminative model. The former produces synthetic data given some noise source by learning the distribution and features of true historical samples, while the latter is similar to a classifier that distinguishes real from synthetic scenarios.WGAN [5]//

Additionally, a carbon trading mechanism is leveraged to balance the system economy and environmental friendliness.

Before 2016, research in this field was limited and thereafter its practical usage came into existence worldwide.

As mentioned, the functionality of GAN is based on similar principles of neural networks as a training set has given as input to learning generate novel data that similar to the training set.

This study aims to explore the effective management of distributed renewable energy in the comprehensive energy system of multi user parks. The remainder of this paper is organized as follows. Section 2 introduces the framework of virtual power plant. Section 3 illustrates the wind forecast error labeling model based on agglomerative clustering algorithm. Section 4 proposes and describes the WGAN-GP based scenario generation model detail. Results are discussed and evaluated in Section 5. Section 6 provides our conclusion.

2 The framework of virtual power plant

This paper focuses on coordinating the combined cooling, and electricity integrated with PV technology. According to the characteristics of PIESs, we will design the operation framework of VPP and analyze the characteristics of various resources in VPP. To show the proposed VPP, it first introduces the overall framework of VPP, and then shows how each of its equipment units were modeled.

2.1 Physical model of VPP

In this study, the proposed VPP encompasses various types of distributed energy sources and loads of differing capacities, and its architecture is depicted in Fig. 1. Specifically, the system studied comprises of two PIESs, covering two forms of energy: electrical load (EL) and cooling load (CL). Electrical energy is equipped with PV, ESS, the micro-turbine generator (MTG) and the main grid, while cold energy comes from energy converter equipment such as electric chillers (EC) to generate cooling for the system.

Here, the main components of REs are rooftop PV module, which can convert and generate power, and cooling for end users. Electricity and cooling loads are respectively the power load and the building heat load of the industrial park. In order to ensure the safe, flexible and economical operation of the system, buffer devices such as energy storage system (ESS) are also configured. Meanwhile, each PIES is connected through power lines and can interact with the external power grid.

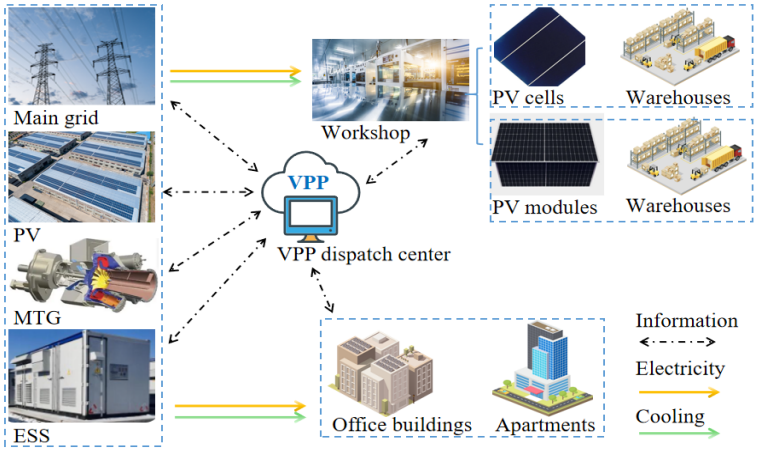

Fig. 1. Basic structure of virtual power plant (VPP)

2.2 Overall structure of VPP system

As mentioned earlier, the VPP system aggregates industrial user load, residential user load, distributed photovoltaic, distributed energy storage for operation. It is modeled to integrate these components to meet the demands and minimize operating costs and carbon emissions. It is assumed that PV take precedence in fulfilling the power load demand, with any remaining demand being met by the main grid and MTG.

VPP units are managed and coordinated by a centralized energy information management system, which can manage and work together across different geographic / electrical locations and technology types to meet user load requirements. Among them, there are two sources of uncertainty that we consider, namely, the PVs output and the load demands. Reducing the impact of uncertainties on scheduling results is the focus of the differential modeling of uncertainties.

For the output of PVs, it mainly depends on external weather, especially solar radiation and cloudiness. To overcome the uncertainty of PVs, scholars put forward the probability density function (PDF) of PV to estimate. For the loads, we consider adjusting electricity consumption based on integrated demand response (IDR) to further mitigate the adverse effects of high power generation on electricity prices, operating costs. Note that the cooling load is composed of an air conditioning system, which injects cold

air into the surrounding environment to reduce temperature, thereby meeting the temperature range required by different workshops, office buildings, residential buildings, and other buildings in the park. It is commonly modeled based on the temperature and thermodynamic models of the building.

Currently, stochastic programming and robust optimization are two common approaches to dealing with the uncertainties of PVs output and cooling load. Although PVs output and loads characteristics have been studied, it is difficult to overcome the drawbacks of the above two methods in practical applications. In this study, historical data will be utilized for appropriate analysis through deep learning methods. For uncertainties, historical data will be used for proper analysis through deep learning methods in this study. In addition, this work assumes that VPP participates in carbon trading to reduce emissions, forcing PIES to use less-pollutant energy through an emission cost model with penalty factors.

2.3 Analysis of PIES characteristics

Focus first on price-based demand response (DR), which can leverage the demand side as an alternative power source to the supply side. Then consider the plant production constraints related to load, as well as cooling models for buildings in industrial parks. Finally, analyze the uncertainty of PV power generation.

Demand response (1) Electric load model.

Flexible electricity loads help reduce operating costs. It comes from loads that can be reduced or transferred from industrial and residential buildings. Ensure that the total electricity demand is met, the electricity consumption cycle can be flexibly adjusted through price guidance. Note that the integration DR cost of integration is made up of compensation costs for transferable loads (TLs) and interruptible loads (ILs). Eqs. (1)-(4) illustrates that TLs can be transferred from peak hours to off-peak hours to achieve the purpose of peak load and valley filling. The TLs quantity after a response can be expressed as the load on the input minus the load on the output. ILs means that customers reduce the portion of loads based on the rigidity of electricity consumption and incentive measures, expressed by the formula (6)-(9). In brief, the electrical load in period t can be described as follows:

$$P_{t,\min}^{\text{TL, in}} \leq P_t^{\text{TL, in}} \eta_t^{\text{TL, in}} \leq P_{t,\max}^{\text{TL, in}}, \forall t \in T \tag{1}$$

$$P_{t,\min}^{\text{TL, out}} \leq P_t^{\text{TL, out}} \eta_t^{\text{TL, out}} \leq P_{t,\max}^{\text{TL, out}}, \forall t \in T \tag{2}$$

$$\eta_t^{\text{TL, in}} + \eta_t^{\text{TL, out}} \leq 1, \forall t \in T \tag{3}$$

$$\sum_{t=1}^{T} P_t^{\text{TL, in}} - \sum_{t=1}^{T} P_t^{\text{TL, out}} = 0 \tag{4}$$

$$0 \leq P_t^{\text{IL}} \leq P_{t,\max}^{\text{IL}}, \forall t \in T \tag{5}$$

where $t \in \{1, \cdots, T\}$, and T is the total number of periods in a scheduling cycle, which is set to $24h$. $\eta_t^{\text{TL, in}}, \eta_t^{\text{TL, out}} \in \{0, 1\}$. When considering DR as flexible, the $P_t^{\text{TL, in}}$ and $P_t^{\text{TL, out}}$ limitation based on maximum and minimum allowable TL quantities

transferred in or out of load (kW) at time t, expressed as $P^{\text{TL, in}}_{t,\max}$, $P^{\text{TL, in}}_{t,\min}$, $P^{\text{TL, out}}_{t,\max}$ and $P^{\text{TL, out}}_{t,\min}$ respectively. Similarly, $P^{\text{IL}}_{t,\max}$. In this study, $P^{\text{IL}}_{t,\max}$ is assumed to be 10% of the electrical load demand in each period.

$$P_{\text{load},t} = P^0_{\text{load},t} + P^{\text{TL, in}}_t - P^{\text{TL, out}}_t - P^{\text{IL}}_t, \forall t \in T \tag{6}$$

where $P_{\text{load},t}$ and $P^0_{\text{load},t}$ imply the actual and initial power loads in period t, respectively.

(2) Flexible cooling loads.

Similar to heat load, temperature plays a substantial role in the assessment of meeting heating demand. The cooling load concerned in this paper is composed of air conditioning system. Taking photovoltaic industrial park as an example, the mathematical modeling of cooling load is constructed based on thermodynamic model considering the characteristics of the park.

Note that PV industry chain refers to a series of links, including the production of silicon materials and wafers in the upstream, the manufacturing of PV cells and PV modules in the midstream, and the construction and operation of photovoltaic power plants in the downstream. Especially in the production process, different production processes have different requirements for indoor temperature in the factory building. Here, we focus on the midstream, and corresponding workshops are represented by set W. Specifically, the buildings involved are divided into two categories: production workshops $w \in W$, apartment and office buildings $w' \in W$. For the production workshop, the mathematical modeling of the building temperature at each hour is obtained by [7, 8].

$$\mathcal{T}^{\text{in},c}_{t,w} = \mathcal{T}^{\text{in},c}_{t-1,w} e^{\frac{-\Delta t}{\tau}} + (\mathcal{T}^{\text{out},c}_{t-1,w} - \tilde{C}^c_{t-1,w} R)(1 - e^{\frac{-\Delta t}{\tau}}), \forall t \in T, w \in W \tag{7}$$

$$\tilde{C}^c_{t-1,w} = \left(\mathcal{T}^{\text{out},c}_{t-1,w} - \frac{\mathcal{T}^{\text{in},c}_{t,w} - \mathcal{T}^{\text{in},c}_{t-1,w} e^{\frac{-\Delta t}{\tau}}}{1 - e^{\frac{-\Delta t}{\tau}}} \right) \frac{1}{R}, \forall t \in T, w \in W \tag{8}$$

where $\tilde{C}^c_{t-1,w}$ indicates the injected cooling air to the building at period $t-1$ which is the conversion form of Eq. (8). Obviously, Eq. (7) demonstrates that the indoor temperature for the previous hour $\mathcal{T}^{\text{in},c}_{t-1,w}$ has a direct relation to the current indoor temperature $\mathcal{T}^{\text{in},c}_{t,w}$. The outdoor temperature in period t is $\mathcal{T}^{\text{out},c}_{t,w}$, $\Delta t = 1(h)$ and R is the thermal resistance of the house shell. Note that $\tau = RC^{\text{air}}$ where C^{air} is the heat capacity of the indoor air.

For the apartment and office buildings, we introduce another thermal modeling [11] based on the predicted mean vote (PMV) which to quantify the users acceptable thermal comfort range more accurately. The cooling load in the building is calculated as follows:

$$\tilde{C}^c_{t-1,w'} = \frac{(\mathcal{T}^{\text{out},c}_{t,w'} - \mathcal{T}^{\text{in},c}_{t-1,w'}) + \frac{KF(\mathcal{T}^{\text{out},c}_{t,w'} - \mathcal{T}^{\text{in},c}_{t-1,w'})}{C^{\text{air}} d^{\text{air}} V} \Delta t}{\frac{1}{KF} + \frac{1}{C^{\text{air}} d^{\text{air}} V} \Delta t}, \forall t \in T, w' \in W \tag{9}$$

$$PMV = 2.43 - \frac{3.76(\mathcal{T}^{\text{in},a}_{w'} - \mathcal{T}^{\text{in},c}_{w'}(t))}{H(I_{\text{cl}} + 0.1)}, \forall t \in T, w' \in W \tag{10}$$

$$|PMV| \leq \begin{cases} 0.9, t \in [1:00 - 7:00] \cup [20:00 - 24:00]; \\ 0.5, t \in [8:00 - 19:00] \end{cases} \tag{11}$$

where K is the comprehensive heat transfer coefficient of the building; F and V are the surface area and volume of the building, respectively; The density of indoor air is expressed in d^{air}; The human energy metabolism rate and the thermal resistance of clothing are denoted as H and I_{cl}, respectively; $\mathcal{T}_{\tilde{w}}^{\text{in},a}$ is the average temperature of human skin in a comfortable state. To ensure user comfort, Eq. (11) shows the PMV limits in Eq. (10) are given according to the ISO-7730 standard.

Eqs. (8-9) indicate the forecasted cooling air energy when customers demand to set the temperature at a specific amount. According to the characteristics of the above two types of buildings, the temperature could vary between an allowable range as in Eq.(12).

$$\mathcal{T}_{t,\tilde{w},\min}^{\text{in},c} \leq \mathcal{T}_{t,\tilde{w}}^{\text{in},c} \leq \mathcal{T}_{t,\tilde{w},\max}^{\text{in},c}, \forall \tilde{w} \in W, \forall t \in \{1, \cdots, T\} \tag{12}$$

Therefore, in case of flexible cooling loads, the reduction of the cooling load cannot exceed its upper limit.

$$0 \leq C_{t,\tilde{w}}^{\text{IL},c} \leq C_{t,\tilde{w},\max}^{\text{IL},c}, \forall \tilde{w} \in W \tag{13}$$

$$C_t^{\text{IL},c} = \left| \sum_{\tilde{w}} C_{t,\tilde{w}}^{c} - \sum_{\tilde{w}} \tilde{C}_{t,\tilde{w}}^{c} \right| + \sum_{\tilde{w}} C_{t,\tilde{w}}^{\text{IL},c}, \forall \tilde{w} \in W \tag{14}$$

$$C_{\text{load},t}^{c} = C_{\text{load},t}^{\text{IL},c,0} - \sum_{\tilde{w}} C_{t,\tilde{w}}^{\text{IL},c}, \forall t \in T, \forall \tilde{w} \in W \tag{15}$$

where Eq. (13) illustrates the fluctuation range of the interrupted cooling power; Eq. (14) states the deviation from the desired cooling power and the cuttable cooling load of building $\tilde{w}$ during period t; Eq. (15), $C_{\text{load},t,\tilde{w}}^{\text{IL},c,0}$ and $C_{\text{load},t,\tilde{w}}^{\text{IL},c}$ represent the cooling load demand before and after the reduction for each building, respectively.

Productive maintenance Pay attention to the two types of workshops mentioned above: PV cell processing and module encapsulation, each with n_c and n_m production lines. Moreover, the production of the two workshops must be carried out in strict accordance with the predetermined production sequence. Each workshop is equipped with a warehouse to store the products already produced and to serve as a buffer between the two. Under the premise of meeting diversified orders (PV cell orders, PV module orders, etc.), in order to maximize production line productivity, when some PV cells are produced, they should be put into the PV module production line for processing as soon as possible. Taking the production of PV modules as an example in Eqs. (16-17), the process flow of PV modules preparation include cells classification, jointing, layering, laminating, EL testing, framing, wiring, PV cleanning, IV testing, finished product inspection, packaging and storage, etc. Next, we analyze the key factors that affect production maintenance in VPP system.

$$\bar{F}_m = \sum_{t=h}^{T} \sum_{m=1}^{n_m} v_{m,t} F_m, \forall h \in T \tag{16}$$

$$T_{m,\min} \leq \sum_{t=h}^{T} v_{m,t} \leq T_{m,\max}, \forall m \in \{1, ..., n_m\} \tag{17}$$

$$\sum_{t=1}^{h+a} \sum_{cp=1}^{n_{\text{cp}}} v_{\text{cp, t}} F_{\text{cp}} G_{\text{cp}} \leq \sum_{t=1}^{h} \sum_{c=1}^{n_c} v_{c,t} F_c, \forall h \in T \tag{18}$$

$$\sum_{t=1}^{h+b} \sum_{m=1}^{n_m} v_{m,t} F_m \leq \sum_{t=1}^{h} \sum_{\text{cp}=1}^{n_{\text{cp}}} v_{\text{cp},t} F_{\text{cp}} G_{\text{cp}}, \forall h \in T \tag{19}$$

$$\sum_{t=1}^{h+1} \sum_{\text{mp}=1}^{n_{\text{mp}}} v_{\text{mp},t} F_{\text{mp}} G_{\text{mp}} \leq \sum_{t=1}^{h} \sum_{m=1}^{n_m} v_{m,t} F_m, \forall h \in T \tag{20}$$

$$S_{c,\min} \leq S_{t,c} \leq S_{c,\max}, \forall t \in T \tag{21}$$

$$S_{m,\min} \leq S_{t,m} \leq S_{m,\max}, \forall t \in T \tag{22}$$

$$S_{t,c} = S_{t-1,c} + \sum_{c=1}^{n_c} v_{c,t} F_c - \sum_{\text{cp}=1}^{n_{\text{cp}}} v_{\text{cp},t} F_{\text{cp}} G_{\text{cp}}, \forall t \in T \tag{23}$$

$$S_{t,m} = S_{t-1,m} + \sum_{\text{mp}=1}^{n_{\text{mp}}} v_{\text{mp},t} F_{\text{mp}} G_{\text{mp}} - \sum_{m=1}^{n_m} v_{m,t} F_m, \forall t \in T \tag{24}$$

where $n_c = n_{\text{cp}}$, $n_m = n_{\text{mp}}$, F_m is the output per unit time of each PV module production lines, F_{mp} is the packaging quantity per unit time of the corresponding PV module production line, and G_{mp} is the number of PV module in each package; $v_{m,t}, v_{\text{mp},t} \in \{0, 1\}$ are the operating variables of the production line at time t, and when the value is 1, it indicates that the machine is running. Similarly, we define the symbols $F_c, F_{\text{cp}}, G_{\text{cp}}, v_{m,t}$ and $v_{\text{mp},t}$. The inventory status of the PV cells workshop at period t denote as $S_{t,c}$. $S_{c,\min}/S_{m,\min}$ and $S_{c,\max}/S_{m,\max}$ are the minimum and maximum capacities of warehouses corresponding to PV cells and PV modules, respectively. a and b represent the sum of the production time of the PV cells/modules production line and the minimum waiting time of the PV cell/module warehouse, respectively. Eqs. (16-17) indicate production line task constraints, Eqs. (18-20) describe the production sequence: PV cell production line – PV cell packaging – PV module production line – PV module packaging, and two storage status in Eqs. (21-24).

Setting symbols C_c, C_m, C_{cp} and C_{mp} are the operation and maintenance costs involved in each production line of the above four links respectively. In summary, the production maintenance cost in period t can be derived as follows:

$$C_{M,t} = \sum_{c=1}^{n_c} (v_{c,t} C_c) + \sum_{m=1}^{n_m} (v_{m,t} C_m) + \sum_{\text{cp}=1}^{n_{\text{cp}}} (v_{\text{cp},t} C_{\text{cp}}) + \sum_{\text{mp}=1}^{n_{\text{mp}}} (v_{\text{mp},t} C_{\text{mp}}). \tag{25}$$

The power generation cost of photovoltaic units The output of PV is greatly affected by environmental changes such as irradiation intensity, with strong randomness and volatility. Considering the cost of PV power generation, it mainly includes two terms: maintenance costs for PV production and penalty costs for curtailing PV. We know that the irradiation intensity is the most important factor affecting PV output power. To estimate the uncertainties of PV output, the Beta probability density function (PDF) is introduced to describe the irradiance distribution at specific locations, and to further calculate it [1].Solar irradiation is mainly responsible for generating power from a PV generator. The beta distribution is commonly used to model the solar irradiation. The PDF of beta distribution function in period t is represented as:

$$f(\theta_t) = \begin{cases} \frac{\Gamma(\alpha+\beta)}{\Gamma(\alpha)+\Gamma(\beta)}\theta_t^{\alpha-1}(1-\theta_t)^{\beta-1}, & 0 \le \theta_t \le 1, \alpha, \beta \ge 0 \\ 0, & \text{otherwise} \end{cases} \tag{26}$$

$$\beta = (1-\mu)\left(\frac{u(1+\mu)}{\sigma^2} - 1\right), \alpha = \frac{\mu\beta}{1-u} \tag{27}$$

$$p(\theta_t) = \int_{\theta_c}^{\theta_d} f(\theta_t) d\theta_t, \forall t \in T \tag{28}$$

$$\tilde{P}_t^{\text{PV}} = \eta_{\text{PV}} F_{\text{PV}} \theta_t, \forall t \in T \tag{29}$$

$$C_{\text{loss},t}^{\text{PV}} = \varepsilon_{\text{re}}^{\text{PV}} |P_t^{\text{PV}} - \tilde{P}_t^{\text{PV}}| + \varepsilon_{\text{ge}}^{\text{PV}} P_t^{\text{PV}}, \forall t \in T \tag{30}$$

where β and α in Eq.(26) denote the mean and standard deviation of the irradiance to calculate the parameters of the Beta PDF which are given in Eq.(27). η_{PV} is the efficiency of PV, F_{PV} denote the total area of PV and θ_t solar irradiance at time t. ε_{re} and ε_{ge} are the unit penalty cost for curtailing PV and the maintenance cost per unit of production respectively. The probability of solar irradiance state θ_t can be calculated in Eq. (28). Then, we can calculate the PV output as shown in Eq. (29). Therefore, the loss of PV can be calculated by Eq. (30).

3 Deep learning and clustering algorithms for source-side and load-side uncertainties

GAN theory emanate in the category of machine learning frameworks, which are powerful generative models. In this section, variations of GAN are introduced into different scene generation tasks for PIES. Firstly, we introduce the framework of WGAN-GP, and then provide a scenario reduction method to get typical scenes and reduce computational complexity.

3.1 WGAN-GP

To enhance the authenticity, we utilize the trained Wasserstein generative adversarial network with gradient penalty (WGAN-GP) to generate the scenario of PVs output and cooling load. WGAN-GP is a variant of the GAN that employs the Wasserstein distance instead of the Jensen-Shannon divergence for measuring the dissimilarity between the

generated and actual data distributions. For ease of understanding, the GAN architecture is introduced first.

In general, the input of GAN consists of two groups of data, one is noise vectors z, and the other is historical data x with probability $\mathbb{P}_x$. The training process of GAN is completed by two game networks, namely generator G and discriminator D. Technically, D is trained iteratively with G. In the original GAN theory, both G and D are not required to be neural networks, only functions that can fit the corresponding generation and discrimination. We set G and D as deep neural networks θ_G and θ_D respectively to ensure the reliability of the experimental results

During training, both can continuously improve performance through an iterative adversarial process. Indeed, the task of G is to learn the generators distribution over real data x to maximize the interference with the discriminator. The training data z satisfying any prior $\mathbb{P}_z$ is input into G, then represent a mapping to data space as $G(z;\theta_G)$, where $G(\cdot)$ is a differentiable function represented by a multilayer perceptron with the trained network parameters θ_G. This means that G implicitly defines a probability distribution of the sample $G(z)$ obtained when taking a batch z of inputs from $\mathbb{P}_z$. D aims to maximize the probability of assigning the correct label to both training examples and samples from G. We also define a second multilayer perceptron $D(x;\theta_D)$ that outputs a single scalar. By varying θ_D, the distribution of z can be changed to be as close as possible to $\mathbb{P}_x$ until it can't distinguish whether the sample is from a generator or historical training data. Therefore, the loss functions [4] for both networks can be defined as

$$L_G = \mathbb{E}_{z\sim\mathbb{P}_z}[\log(1-D(G(z)))], L_D = \mathbb{E}_{x\sim\mathbb{P}_x}[\log D(x)]+\mathbb{E}_{z\sim\mathbb{P}_z}[\log(1-D(G(z)))],$$

where $G(z)$ represents the sample generated by G, and $D(\cdot)$ denotes an output of D.

In summary, a dynamic minmax two-player game is built between G and D, where they play against each other and learn from each other and ultimately reach a state of Nash equilibrium. To some extent the generator is trained to fool the discriminator. Formally, the game is the minimax objective [6]:

$$\min_G \max_D \mathop{\mathbb{E}}_{x\sim\mathbb{P}_x}[\log D(x)] + \mathop{\mathbb{E}}_{z\sim\mathbb{P}_z}[\log(1-D(G(z)))].$$

The Wasserstein distance (or earth mover distance) measures the difference between the distribution of real data and synthetic data directly [5].

$$\mathbb{W}(\mathbb{P}_x,\mathbb{P}_g) = \sup_{\|D\|_L\leq 1} \mathop{\mathbb{E}}_{x\sim\mathbb{P}_x}[D(x)] - \mathop{\mathbb{E}}_{\tilde{x}\sim\mathbb{P}_g}[D(\tilde{x})],$$

where the supremum is over all the 1-Lipschitz functions $D(\cdot)$ following this constraint: $|D(x_1)-D(x_2)|\leq|x_1-x_2|$, and $\mathbb{P}_g$ is once again the model distribution implicitly defined by $\tilde{x}=G(z)$.

WGAN-GP is also consisted of G and D. It aims to address some of the limitations of the original GAN, such as gradient vanishing and training instability. In more detail, we apply a soft version of the constraint on the gradient norm of the random sample $\hat{x}\sim P_{\hat{x}}$, i.e. a gradient penalty term is introduced into the discriminator loss function, which can ensure that the discriminator approximately satisfies 1-Lipschitz continuity. The

gradient penalty is given by: $\mathbb{E}_{\hat{x}\sim\mathbb{P}_{\hat{x}}}\left[(\|\nabla_{\hat{x}}D(\hat{x})\|_2-1)^2\right]$, where $\hat{x}=\varepsilon x+(1-G(z))$, it is homogeneous sampling points on the link between x and z, ε is a random number that satisfies $\varepsilon\sim[0,1]$. The objective function of D can be reformulated as [5]:

$$\mathcal{L}_D=\mathop{\mathbb{E}}_{\tilde{x}\sim\mathbb{P}_g}[D(\tilde{x})]-\mathop{\mathbb{E}}_{x\sim\mathbb{P}_x}[D(x)]+\lambda\mathop{\mathbb{E}}_{\hat{x}\sim\mathbb{P}_{\hat{x}}}\left[(\|\nabla_{\hat{x}}D(\hat{x})\|_2-1)^2\right],$$

where $\|\cdot\|_2$ represents the 2-norm, λ is the gradient penalty coefficient. $P_{\hat{x}}$ is defined as uniformly sampling along a straight line between the point pairs sampled from $\mathbb{P}_x$ and $\mathbb{P}_g$. Next, we will provide a detailed training process for WGAN-GP.

Algorithm 1 The training processes of WGAN-GP.

Input: The random noise vectors with distribution $\mathbb{P}_z$, set of historical data with distribution $\mathbb{P}_d$, the number of discriminator iterations per generator iteration n_D, the number of iterations n_{it}, Adam hyperparameters α,β_1,β_2. positive integers t, n and m, the penalty coefficient λ.
Output: Parameters θ_D and θ_G.

Set $\alpha=,\beta_1=,\beta_2=$.
Initialize discriminator parameters θ_{D0}, initial generator parameters θ_{G0}.
for $n_{it}=1,\cdots,t$ **do**
  for $n_D=1,\cdots,n$ **do**
    Sample $\{z^i\}_{i=1}^m\sim\mathbb{P}_z$ a batch of noise priors, $\{x^i\}_{i=1}^m\sim\mathbb{P}_x$ from database, $\varepsilon\sim U[0,1]$.
    $\tilde{x}\leftarrow G(z,\theta_G)$, where $\tilde{x}=\{\tilde{x}^i\}_{i=1}^m$, $z=\{z^i\}_{i=1}^m$.
    $\hat{x}\leftarrow\varepsilon x+(1-G(z))$, where $\hat{x}=\{\hat{x}^i\}_{i=1}^m$, $x=\{x^i\}_{i=1}^m$.
    $\mathcal{L}_D^i\leftarrow D_{\theta_D}(\tilde{x})-D_{\theta_D}(x)+\lambda(\|\nabla_{\hat{x}}D_{\theta_D}(\hat{x})\|_2-1)^2$.
    $\theta_D\leftarrow Adam\left(\nabla_{\theta_D}\frac{1}{m}\sum_{i=1}^m\mathcal{L}_D^i,\theta_D,\alpha,\beta_1,\beta_2\right)$.
  end for
  Sample $\{z^i\}_{i=1}^m\sim\mathbb{P}_z$.
  $\theta_G\leftarrow Adam\left(\nabla_{\theta_G}\frac{1}{m}\sum_{i=1}^m(-G(z^i,\theta_G)),\theta_G,\alpha,\beta_1,\beta_2\right)$.
end for

3.2 Uncertainty simulation

For the traditional optimization approsch, there are usually two methods used to derive the unknown distribution of data. One is the stochastic optimization method, which assumes that the uncertain output follows a certain distribution, i.e. selecting this distribution as the best fit distribution for historical data, and then generating possible real-world scenarios based on sampling methods; Another is robust, which uses limited data to describe deterministic uncertainty sets or zero historical data information if the uncertainty set is defined based on expert experience. However, in practice, due to limited data volume, there may be deviations in the distribution derived from the former, leading to suboptimal solutions, while the latter is very conservative. To make the probability distribution closer to the real data, this paper uses a method related to robust optimization of distribution, where the true distribution of random variables is unknown and assumed to be in a confidence set [15].

In our method, we start from a given historical data set, use WGAN-GP method to train the historical data to obtain the classical scenario, and then construct a confidence set for the unknown probability distribution by statistical inference technique. In detail, the uncertainty simulation includes two steps: scenario generation and scenario reduction. We first use WGAN-GP to generate scenarios, and then the k-means++ algorithm is used to cluster a large number of scenarios generated by a WGAN-GP to obtain typical scenarios.

Concretely, given a set of historical data, the trained WGAN-GP generates N PV outputs and N cooling load scenarios, so there are N^2 combinations. As N increases, the number of combined scenes grows exponentially, bringing considerable computational complexity. Hence, a scenario reduction method is proposed, which uses the k-means++ algorithm to make a balance computational complexity and reliability, as the computational performance of stochastic programming optimization models highly depends on the size of the scenario set. We also introduce typical internal validity indexes such as the Davis Burdin index (DBI) and Silhouette Coefficient (SC), which are widely used in research on the correlation of multi-wind farms and classification of load curves [19], for quantitative analysis.

After the above scenarios are reduced, the scenario probability distribution obtained by scenario clustering has a certain error. Set p_s as the probability value of the discrete scenario $s \in \mathbf{S}$, $|\mathbf{S}| = N_s$, and M is the number of historical data samples.

To obtain the worst probability distribution of each discrete scenario, we utilize composite-norm to define an uncertainty confidence set Ω^p based on a given confidence level and the amount of available historical data, which satisfies a probability distribution expressed as:

$$\Omega^p = \left\{ \{p_s\} \middle| \sum_{s=1}^{N_s} p_s = 1, \sum_{s=1}^{N_s} |p_s - p_{s0}| \le \theta_1, \max_{1 \le s \le N_s} |p_s - p_{s0}| \le \theta_\infty \right\}, \quad (31)$$

where $p_{s0} = |s|/M$ as the initial probability with $M = \sum_{s=1}^{N_s} |s|$, $|s|$ indicate the number of the occurrences of scenario s. Note the confidence levels that Eq.(31) needs to meet: $\alpha_1 = 1 - 2N_s e^{-\frac{2M\theta_1}{N_s}} \frac{-b \pm \sqrt{b^2-4ac}}{2a}$ for l_1 norm, $\alpha_\infty = 1 - 2N_s e^{-\frac{2M\theta_1}{N_s}}$ for l_∞ norm. Indeed, parameters θ_1 and θ_∞ are the one-sided upper confidence limits corresponding to l_1 and l_∞ norms, respectively, represented as $\theta_1 = \frac{N_s}{2M} \ln \frac{2N_s}{1-\alpha_1}$ and $\theta_\infty = \frac{1}{2M} \ln \frac{2N_s}{1-\alpha_\infty}$.

Besides, observing Eq. (31), the comprehensive norm confidence interval contains absolute value constraints. Therefore, it is necessary to use the method in [11] to introduce 0-1 variables for linearization and equivalent transformation. After the entire process mentioned above, we ultimately obtained p_S is the real scenario probability.

4 Optimization model of the VPP

To coordinate the integrated demand response and uncertainty of RIES, a data-driven two-stage distributionally robust optimization (2-DRO) model is proposed for the VPP, with the overall objective of minimizing VPP operation cost.

4.1 Objective function

(1) The first stage: It mainly considers the start-up and shutdown costs of MTG and the maintenance costs of machines in the workshop, expressed as $U_i, D_i, i \in \{1, 2, \cdots, n_G\}$, where n_G is the number of MTGs. The switch status flag of MTG is represented by binary variables $y_{i,t}$, $z_{i,t}$, and the specific expressions is shown in Eq.(35), that is, when $y_{i,t}$ and $z_{i,t}$ take a value of 0, it indicate MTG is open/off, otherwise 0. Assume that the symbol n_G is the number of is and T is the scheduling period. and the production maintenance cost $C_{M,t}$, Therefore, the objective function is described as follows:

$$\min \sum_{t=1}^{T} \left(\sum_{i=1}^{n_G} (U_i y_{i,t} + D_i z_{i,t}) + C_{M,t} \right). \tag{32}$$

(2) The second stage: It mainly consists of seven components, such as solar curtailment cost C_{loss}, MTG operating cost C_{MTG}, ESS operating cost C_{ESS}, CO_2 emission penalty cost C_{CO_2}, DR compensation cost C_{DR} for shifting their loads, the purchase power costs from grid C^b_{gr}, and the revenue from selling electricity to grid C^s_{gr}, which are presented in (33).

$$\min \left(C_{\text{MTG}} + C_{\text{ESS}} + C_{CO_2} + C_{\text{DR}} + C_{\text{loss}} + C^b_{\text{gr}} - C^s_{\text{gr}} \right). \tag{33}$$

The specific formulas for these are as follows:

$$C_{\text{MTG}} = \sum_{t=1}^{T} \sum_{i=1}^{n_G} \left(a_i P^{\text{MTG}}_{i,t} + b_i u^{\text{MTG}}_{i,t} \right)$$

$$C_{\text{ESS}} = \sum_{t=1}^{T} \left(\varepsilon_{\text{ESS}} (P^{\text{ESS}}_{\text{ch},t} + P^{\text{ESS}}_{\text{dc},t}) \right)$$

$$C_{CO_2} = \varepsilon_{CO_2} \sum_{t=1}^{T} \left(k_{\text{MTG}} \sum_{i=1}^{n_G} P^{\text{MTG}}_{i,t} + k_{\text{gr}} P^{b}_{\text{gr},t} \right)$$

$$C_{\text{DR}} = \sum_{t=1}^{T} \left(\rho^{\text{TL}} P^{\text{TL, in}}_{t} + \rho^{\text{IL}} P^{\text{IL}}_{t} + \rho^{c} C^{\text{IL},c}_{t} \right)$$

$$C^b_{\text{gr}} = \sum_{t=1}^{T} \varepsilon^b_{\text{gr}} P^b_{\text{gr},t}$$

$$C^s_{\text{gr}} = \sum_{t=1}^{T} \varepsilon^s_{\text{gr}} P^s_{\text{gr},t}$$

$$C_{\text{loss}} = \sum_{t=1}^{T} C^{\text{PV}}_{\text{loss},t}$$

where a_i and b_i represent the primary term and constant term coefficients of the MTG operation cost, respectively; ε_{ESS} denotes the unit-price of ESS charging and discharging operation; ε_{CO_2} is the unit penalty cost for curtailing PV, k_{MTG} and k_{gr} are the CO_2

emissions per unit electricity produced by the MTG and the grid, respectively; ρ^c describes the flexible cooling compensation price for interruption cooling loads, Similar, ρ^{TL} and ρ^{IL} are flexible TL/IL compensation prices for electric loads; $\varepsilon^b_{\text{gr}}$ and $\varepsilon^s_{\text{gr}}$ indicate the unit price of electricity purchased and sold by PIES to the grid. $P^{\text{MTG}}_{i,t}$ and $u_{i,t}$ quantify the power generation/maintenance tasks of the i-th MTG at time t; $P^{\text{ESS}}_{\text{ch},t}$ and $P^{\text{ESS}}_{\text{dc},t}$ are the charging and discharging powers of the ESS, respectively; $P^b_{\text{gr},t}$ and $P^s_{\text{gr},t}$ respectively quantify the powers purchased and sold by PIES from and to the main grid in period t.

4.2 Constraints

This section will introduce all other constraints in the VPP system except for DR, PV unit power generation sets and the production maintenance. They can be derived as follows:

$$0 \le P^{\text{MTG}}_{i,t} \le \eta^{\text{MTG}}_{i,t} P^{\text{MTG}}_{i,\max}, \forall i \in \{1,2,\cdots,n_G\}, \forall t \in T \quad (34)$$

$$y_{i,t} + z_{i,t} \le 1, \forall i \in \{1,2,\cdots,n_G\}, \forall t \in T \quad (35)$$

$$\eta^{\text{MTG}}_{i,t} P^{\text{MTG}}_{i,t+1} - \eta^{\text{MTG}}_{i,t+1} P^{\text{MTG}}_{i,t} \le \Delta P^{\text{MTG}}_{U,\max}, \forall i \in \{1,2,\cdots,n_G\}, \forall t \in T \quad (36)$$

$$\eta^{\text{MTG}}_{i,t} P^{\text{MTG}}_{i,t-1} - \eta^{\text{MTG}}_{i,t+1} P^{\text{MTG}}_{i,t} \le \Delta P^{\text{MTG}}_{D,\max}, \forall i \in \{1,2,\cdots,n_G\}, \forall t \in T \quad (37)$$

$$0 \le P^{\text{ESS}}_{\text{ch},t} \le \eta^{\text{ch}}_t P^{\text{ESS}}_{\text{ch},\max}, \forall t \in T \quad (38)$$

$$0 \le P^{\text{ESS}}_{\text{dc},t} \le \eta^{\text{dc}}_t P^{\text{ESS}}_{\text{dc},\max}, \forall t \in T \quad (39)$$

$$\eta^{\text{ch}}_t + \eta^{\text{dc}}_t \le 1, \forall t \in T \quad (40)$$

$$C^{\text{ESS}}_{\min} \le C^{\text{ESS}}_0 + e_{\text{ch}} \sum_{t=1}^{T} (P^{\text{ESS}}_{\text{ch},t} \cdot \Delta t) - \frac{1}{e_{\text{dc}}} \sum_{t=1}^{T} (P^{\text{ESS}}_{\text{dc},t} \cdot \Delta t) \le C^{\text{ESS}}_{\max}, \forall t \in T \quad (41)$$

$$C^{\text{ESS}}_0 = C^{\text{ESS}}_{\text{end}} \quad (42)$$

$$P^{\text{PV}}_{\text{ge},t} + P^b_{\text{gr},t} + P^{\text{ESS}}_{\text{dc},t} + \sum_{i=1}^{n_G} P^{\text{MTG}}_{i,t} = P_{\text{load},t} + C^c_{\text{load},t} + P^{\text{ESS}}_{\text{ch},t}, \forall t \in T \quad (43)$$

$$0 \le P^b_{\text{gr},t} \le P^b_{\text{gr},\max}, \forall t \in T \quad (44)$$

$$0 \le P^s_{\text{gr},t} \le P^s_{\text{gr},\max}, \forall t \in T \quad (45)$$

where $P^{\text{MTG}}_{i,t}$ and $P^{\text{MTG}}_{i,t+1}$ are the output power of the i-th MTG in period t and the next period $t+1$, respectively; the maximum power supplied by MTG is $P^{\text{MTG}}_{i,t,\max}$; and $\Delta P^{\text{MTG}}_{U,\max}/\Delta P^{\text{MTG}}_{D,\max}$ are the maximum allowable rates of the MTG climbing / landslide rates. The maximum chargeable/discharging power of ESS is expressed as $P^{\text{ESS}}_{\text{ch},\max}$ and $P^{\text{ESS}}_{\text{dc},\max}$, and its charging / discharging efficiency is e_{ch} and e_{dc}; The minimum and maximum capacities of ESS are denoted by $C^{\text{ESS}}_{\min}$ and $C^{\text{ESS}}_{\max}$. Both $\eta^{\text{MTG}}_{i,t}$ and $\eta^{\text{MTG}}_{i,t+1}$ are $0/1$ variables, which represent the MTG state, if $\eta^{\text{MTG}}_{i,t} = 1$ means the i-th MTG is running, otherwise 0. The operating state of ESS uses the Boolean variables η^{ch}_t and η^{dc}_t. If $\eta^{\text{ch}}_t = 1$ or $\eta^{\text{dc}}_t = 1$, indicating that ESS is in charge or discharge state.

Among them, Eqs.(34-37) express the output and the ramping constraints of MTG; Ess operational constraints are represented by constraints (38-42), which corresponding to avoiding ESS overcharge/discharge as described by Eq. (41), and the remaining capacity of ESS described by Eq.(42) should remain the same at the beginning and end of each scheduling cycle; The formula (43) maintain the power supply and demand balance of VPP system in scenario s during the t-time period; The interaction constraints between PIES and the main power grid are reflected in inequalities Eqs.(44-45).

5 Model transformation and solution

To solve the proposed 2-DRO model, we first convert the above model into a min-max-min structure, and then use the inexact column-and-constraint generation (IC&CG) algorithm to solve it.

5.1 Model solution strategy

As mentioned above, in the 2-DRO scheduling model, the first stage develops the operational status strategy of the components, including MTG, ESS, and the machines in the plant, which is characterized by 0-1 integer variables; In the second stage, the dispatching plan is developed after the uncertainty of PV and cooling load demand is revealed, including the output of MTG, the purchase of power from the main grid and the sale of power, etc., and continuous variables are used to characterize them. Therefore, the above decision variables can be expressed as follows:

$$\begin{aligned}\mathbf{U} &= \left[y_{i,t}, z_{i,t}, \eta_t^{\mathrm{dc}}, \eta_t^{\mathrm{ch}}, v_{m,j,t}, v_{\mathrm{mp},j,t}, v_{c,j,t}, v_{\mathrm{cp},j,t}\right] \\ \mathbf{V} &= \left[P_{i,t}^{\mathrm{MTG}}, P_{\mathrm{ch},t}^{\mathrm{ESS}}, P_{\mathrm{dc},t}^{\mathrm{ESS}}, P_t^{\mathrm{PV}}, P_{\mathrm{gr},t}^{b}, P_{\mathrm{gr},t}^{s}, P_t^{\mathrm{TL}}, P_t^{\mathrm{IL}}, C_{t,\tilde{w}}^{\mathrm{IL},c}\right]\end{aligned} \tag{46}$$

Further, the defined above and described by Eqs. (31)-(44) can be summarized as follows:

$$\begin{aligned}&\min_{u\in\mathbf{U}} \mathbf{A}u + \max_{p_s\in\Omega^p} \sum_{s=1}^{N_s} p_s \min_{v_s\in\mathbf{V}} \mathbf{B}v_s \\ &\text{s. t. } \mathbf{C}u = c, \forall u \in \mathbf{U} \\ &\quad \mathbf{D}u \le d, \forall u \in \mathbf{U} \\ &\quad \mathbf{E}v_s = e, \forall s \in \mathbf{S} \\ &\quad \mathbf{F}v_s \le f, \forall s \in \mathbf{S} \\ &\quad \mathbf{G}u + \mathbf{H}v_s \le g, \forall s \in \mathbf{S}.\end{aligned} \tag{47}$$

where S denotes a collection of scenes, the probability of scenario s after clustering is p_s, and the total number of scenarios is N_s. The term Ω^p denotes the set interval of the scene probability distribution, which is shown in Eq. (31). The bold symbol $\mathbf{A}, \mathbf{B}, \mathbf{C}, \mathbf{D}, \mathbf{E}, \mathbf{F}, \mathbf{G}$, and $\mathbf{H}$ are constant coefficient matrices for the variables under corresponding constraints, c, d, e, f and g are constant column vectors corresponding

to response constraints. The first two lines indicate the MTG/ESS operating state constraints corresponding to Eqs. (35) and (40) of the first stage, and these terms also include constraints on machine state variable in the plant, such as corresponding equations (17-20); The third and fourth parts of the constraints include explicity (34),(36-37),(42) and (44-45), which include constraints of the MTG, ESS capacity, and grid power purchase in the second stage; The fifth line represents the coupling constraints of the decision variables in the two stages, corresponds to the power supply and demand balance constraints described by Eq. (43), and the ESS charge-discharge constraints described by Eqs. (38-39).

Observing the optimal scheduling model, it is undoubtedly very difficult to adopt a direct solution method. Because the model in (47) contains 0-1 integer variables and continuous variables, as well as a min-max-min structure and uncertainty parameters. The wise strategy is to decompose (47) into the master problem (MP) and sub-problem (SP), and then iteratively solve until the given convergence accuracy is achieved. We introduce auxiliary variables γ, $\bar{L}$, and the number of iterations is represented by k. The MP and SP are expressed as follows:

$$
\begin{aligned}
\text{MP:}\quad & \min_{u\in\mathbf{U},\gamma} \ \mathbf{A}u+\gamma \\
& \text{s. t.} \quad \gamma \geq \sum_{s=1}^{N_s} p_s^k \mathbf{B} v_s^k, \forall k \in K, \forall s \in \mathbf{S} \\
& \qquad \mathbf{A}u+\gamma \geq \bar{L} \\
& \qquad \mathbf{C}u = c, \forall u \in \mathbf{U} \\
& \qquad \mathbf{D}u \leq d, \forall u \in \mathbf{U} \\
& \qquad \mathbf{E}v_s^k = e, \forall k \in K, \forall s \in \mathbf{S} \\
& \qquad \mathbf{F}v_s^k \leq f, \forall k \in K, \forall s \in \mathbf{S} \\
& \qquad \mathbf{G}u+\mathbf{H}v_s^k \leq g, \forall k \in K, \forall s \in \mathbf{S}.
\end{aligned}
$$

$$
\begin{aligned}
\text{SP:}\quad & F(u^*) = \max_{p_s\in\Omega^p} \sum_{s=1}^{N_s} p_s^k \min_{v_s\in V} \mathbf{B}v_s^k \\
& \text{s. t.} \quad \mathbf{E}v_s^k = e, \forall k \in K, \forall s \in \mathbf{S} \\
& \qquad \mathbf{F}v_s^k \leq f, \forall k \in K, \forall s \in \mathbf{S} \\
& \qquad \mathbf{G}u^*+\mathbf{H}v_s^k \leq g, \forall k \in K, \forall s \in \mathbf{S}.
\end{aligned}
$$

As mentioned above, as a relaxation of the original problem, MP finds the optimal solution of the first-stage objective function according to the known worst-case probability distribution value, and provides a lower bound LB to the true optimal value. SP is solved under the variable u^* given by the MP and provide the upper bound UB. At the same time, it obtains the worst-case probability distribution of the current iteration and feeds it back to MP for the next iteration.

5.2 Solving algorithm

In this section, we use the IC&CG method to solve the 2-DRO problem, which is a generalization of the C&CG method with an additional valid lower bound constraint. The key difference between the two is that C&CG continuously adds variables and constraints related to SP in MP solving, which results in more compact lower bounds on the original objective function values, leading to fewer iterations. For specific details, see Algorithm 2.

Algorithm 2 ICC&G

1: Initialization: $\bar{L} \leftarrow 0, \bar{U} \leftarrow \infty, \epsilon \in [0,1], \tilde{\epsilon} \in (0, \epsilon/(1+\epsilon)), \{\epsilon_{MP}^k \in (0,1)\}_{k\in K}, \delta \in (0,1), \mathbf{U} \leftarrow \emptyset, k \leftarrow 1, l \leftarrow 0$.
2: **MP solving:**
3: Derive the best feasible solution (u^k, γ^k) within a relative optimality gap of ϵ_{MP}^k. Record LB^k and $UB^k = \mathbf{A}u^k + \gamma^k$.
4: **if** $LB^k > \bar{L}$ **then**
5: $l \leftarrow k$.
6: **end if**
7: $\bar{L} \leftarrow UB^k$
8: **SP solving:**
9: Solve the SP on the basis of the given first-stage varible u^k, obtain the worst probability distribution $p_s^{*,k}$, the second-stage decision varible v_s^k, and SP objective function value $F(u^k)$. Set $\bar{U} = \min\{\bar{U}, \mathbf{A}u^k + F(u^k)\}$.
10: **if** $(\bar{U} - LB^l)/\bar{U} \geq \epsilon$ **then**
11: **if** $(\bar{U} - UB^k)/\bar{U} < \tilde{\epsilon}$ **then**
12: $k \leftarrow l, \bar{L} \leftarrow LB^k, \epsilon_{MP}^k \leftarrow \delta\epsilon_{MP}^k$ for all $k \geq l$, and return to the MP solving phase.
13: **else**
14: $\Omega^p \leftarrow \Omega^p \cup \{p_s^*\}, v_s^k, k \leftarrow k+1$, and go back to the MP solving phase.
15: **end if**
16: **else**
17: Terminates the iteration process and returns u^k.
18: **end if**
19: **return** Output optimal solution.

In Algorithm 2, the MP solving phase allows MP to be solved within a specified relative optimality gap, which is an easy to handle option when solving large-scale or challenging MP in the C&CG method. If LB^k is a valid lower bound, we set l as the current iteration index to indicate that it is the closest iteration with such valid lower bound. It is also equipped with a backtracking routine in step 10-18 that controls the trade-off between bound improvement and inexactness from the MP solving inexactly. As shown in [9], the finite convergence of the algorithm is demonstrated by adjusting the errors such as the actual relative gap $(\bar{U} - LB^l)/\bar{U}$ and the inexact relative gap $(\bar{U} - UB^k)/\bar{U}$ in the backtracking procedure.

6 Case study

6.1 Simulation system and data

Table 1. VPP operating parameters

Parameter	Value	Parameter	Value
$U_i(¥/kW)$	0.25	$D_i(¥/kW)$	0.25
$\varepsilon_{ESS}(¥/kW)$	0.02	$\varepsilon_{re}^{PV}(¥/kW)$	0.62
ε_{ge}^{PV}	*	e_{ch}/e_{dc}	0.95 / 0.95
a_i	1.2	$b_i(¥/kW)$	0.0015
$k_{MTG}(kg/kW)$	0.49	$k_{gr}(kg/kW)$	0.82
ρ^{TL}	*	ρ^{IL}	ρ^{c}
C_c/C_m	*	C_{cp}/C_{mp}	*
$P_{i,\max}^{MTG}(kW)$	300	$P_{ch,\max}^{ESS}/P_{dc,\max}^{ESS}$	$20/20$
$\Delta P_{U,\max}^{MTG}/\Delta P_{D,\max}^{MTG}(kW)$	50 / 50	$P_{gr,\max}^{b}/P_{gr,\max}^{s}(kW)$	600 / 600

Set the time-of-use price of the power grid in this region as follows: for peak period ($9:00C11:0019:00C23:00$), $\varepsilon_{gr} = 1.35(¥/kW)$; for flat period ($8:0012:00C18:00$), $\varepsilon_{gr} = 0.90(¥/kW)$; for valley period ($1:00C7:0024:00$), $\varepsilon_{gr} = 0.48(¥/kW)$.

7 Discussions

According to the characteristics of industrial park, we designed the operating framework of VPP, analyzed the characteristics of various resources of virtual power plant, and built a two-stage distributed robust optimization model.

A multi-energy virtual power plant operation and communication architecture have been established to enable reliable data upload and efficient issuance of control commands.

Acknowledgements

The research is supported by National Key R&DProgram of China (No.2022YFE0196100), and Fundamental Research Grant Scheme (FRGS) of Malaysia(FRGS/1/2022/TK0/UTAR/02/8). The above two grants are also parked under China-Malaysia Intergovernmental Science, Technology and Innovation Cooperative Programme 2023(offer letter MOSTI.700-2/2/8(39), dated 9 February 2023).

References

1. Ju, L., Tan, Z., Yuan, J., Tan, Q., Li, H., Dong, F. A bi-level stochastic scheduling optimization model for a virtual power plant connected to a wind-photovoltaic-energy storage system considering the uncertainty and demand response. Applied energy, 2016, 171: 184-199.
2. Chen, Y., Niu, Y., Du, M., Wang, J. A two-stage robust optimization model for a virtual power plant considering responsiveness-based electric vehicle aggregation. Journal of Cleaner Production, 2023, 405: 136690.
3. Tan, C., Tan, Z., Wang, G., Du, Y., Pu, L., Zhang, R. Business model of virtual power plant considering uncertainty and different levels of market maturity. Journal of Cleaner Production, 2022, 362: 131433.
4. Goodfellow, I., Pouget-Abadie, J., Mirza, M., Xu, B., Warde-Farley, D., Ozair, S., Courville, A., Bengio, Y. Generative adversarial nets. In: Proceedings of the 4th Conference on Neural Information Processing Systems (NIPS), 2014, pp. 1-9.
5. Arjovsky, M., Chintala, S., Bottou, L. Wasserstein generative adversarial networks. In: Proceedings of the 9th International conference on machine learning (ICML), 2017, pp. 214-223.
6. Gulrajani, I., Ahmed, F., Arjovsky, M., Dumoulin, V., Courville, A. C. Improved training of Wasserstein GANs. In: Proceedings of the 31th Conference on Neural Information Processing Systems (NIPS), 2017, pp. 1-11.
7. Tasdighi, M., Ghasemi, H., Rahimi-Kian, A. Residential microgrid scheduling based on smart meters data and temperature dependent thermal load modeling. IEEE Transactions on Smart Grid, 2013, 5(1): 349-357.
8. Saberi-Beglar, K., Zare, K., Seyedi, H., Marzband, M., Nojavan, S. Risk-embedded scheduling of a CCHP integrated with electric vehicle parking lot in a residential energy hub considering flexible thermal and electrical loads. Applied Energy, 2023, 329: 120265.
9. Tsang, M. Y., Shehadeh, K. S., Curtis, F. E. An inexact column-and-constraint generation method to solve two-stage robust optimization problems. Operations Research Letters, 2023, 51(1): 92-98.
10. Mei, S., Tan, Q., Liu, Y., Trivedi, A., Srinivasan, D. Optimal bidding strategy for virtual power plant participating in combined electricity and ancillary services market considering dynamic demand response price and integrated consumption satisfaction. Energy, 2023, 284: 128592.
11. Li, Y., Han, M., Shahidehpour, M., Li, J., Long, C. Data-driven distributionally robust scheduling of community integrated energy systems with uncertain renewable generations considering integrated demand response. Applied Energy, 2023, 335: 120749.
12. Aggarwal, A., Mittal, M., Battineni, G. Generative adversarial network: An overview of theory and applications. International Journal of Information Management Data Insights, 2021, 1(1): 100004.
13. Liu, X. Research on bidding strategy of virtual power plant considering carbon-electricity integrated market mechanism. International Journal of Electrical Power Energy Systems, 2022, 137: 107891.
14. Darvishi, M., Tahmasebi, M., Shokouhmand, E., Pasupuleti, J., Bokoro, P., Raafat, J. S. Optimal operation of sustainable virtual power plant considering the amount of emission in the presence of renewable energy sources and demand response. Sustainability, 2023, 15(14): 11012.
15. Zhao, C., Guan, Y. Data-driven stochastic unit commitment for integrating wind generation. IEEE Transactions on Power Systems, 2015, 31(4): 2587-2596.
16. Chen, Y., Niu, Y., Du, M., Wang, J. A two-stage robust optimization model for a virtual power plant considering responsiveness-based electric vehicle aggregation. Journal of Cleaner Production, 2023, 405: 136690.

17. Gough, M., Santos, S. F., Javadi, M. S., Home-Ortiz, J. M., Castro, R., Catal?o, J. P. Bi-level stochastic energy trading model for technical virtual power plants considering various renewable energy sources, energy storage systems and electric vehicles. Journal of Energy Storage, 2023, 68: 107742.
18. Ju, L., Zhao, R., Tan, Q., Lu, Y., Tan, Q., Wang, W. A multi-objective robust scheduling model and solution algorithm for a novel virtual power plant connected with power-to-gas and gas storage tank considering uncertainty and demand response. Applied Energy, 2019, 250: 1336-1355.
19. Jahangir, H., Tayarani, H., Gougheri, S. S., Golkar, M. A., Ahmadian, A., Elkamel, A. Deep learning-based forecasting approach in smart grids with microclustering and bidirectional LSTM network. IEEE Transactions on Industrial Electronics, 2021, 68(9): 8298-309.